npj | clean water

www.nature.com/npjcleanwater

ARTICLE OPEN

Check for updates

Exploiting interfacial polymerization to fabricate hyper-cross-linked nanofiltration membrane with a constituent linear aliphatic amine for freshwater production

Umair Baig[1] and Abdul Waheed[1]✉

Humanity is facing a global challenge of dwindling water resources and the situation is intensifying due to growing population leading to excessive water pollution. Nanofiltration is an important membrane-based technology for the production of clean and potable water for domestic and industrial setups. Hyper-cross-linked polyamide thin film composite nanofiltration (HCPA-TFC-NF) membranes have been fabricated by using multifunctional amine **1** (possessing two primary -NH_2 and two secondary -NH groups) and bifunctional terephthaloyl chloride **2** (TPC) through interfacial polymerization. The structure of the hyper-cross-linked polyamide network has been successfully confirmed by solid (CP-MAS) ^{13}C NMR, XPS, AFM, FT-IR, elemental mapping, and EDX analysis. The membrane features such as surface morphology and hydrophilicity have been established by FE-SEM and water contact angle measurements. The FE-SEM analysis revealed the formation of uniform polyamide active layer on the surface of PS/PET support, and the pore structure of the membranes was tuned by studying the effect of curing temperature and curing time. The nanofiltration membranes efficiently rejected a series of divalent salts including $MgCl_2$, $CaCl_2$, Na_2SO_4, $MgSO_4$, and NaCl using cross-flow filtration setup. Based on the cross-flow filtration performance, the best conditions for the membrane fabrication were found to be curing temperature of 80 °C with a curing time of 1 h. The highest salt rejection was observed in case of $MgCl_2$ reaching to a value of 98.11% in case of HCPA-TFC-NF@M3 and it was found to be 97.45% in case of HCPA-TFC-NF@M2 while the rejection of $MgCl_2$ was reduced to 94.59% in case HCPA-TFC-NF@M1. HCPA-TFC-NF@M2 showed NaCl rejection of 87.36%. The hydrofluoric acid treatment of HCPA-TFC-NF-M2 increased the water flux while keeping the rejection high. The HCPA-TFC-NF@M2 showed a rejection of >99% for EBT with a permeate flux of 75 LMH.

npj Clean Water (2022)5:46 ; https://doi.org/10.1038/s41545-022-00186-x

INTRODUCTION

The humanity is facing a challenge of water scarcity, which is attributed to rapidly growing population and industrialization. The conventional sources of water coming from glacier melt and rainfall are not enough to meet demands of growing population across the globe[1]. The 40% of world population is already facing severe water crisis, which is estimated to affect 60% of the global population by 2025[2]. Desalination of sea water or brackish water has played a significant role in meeting the demands of water consumption by global population. Currently, there are 15,906 operational desalination plants distributed across 177 countries and these plants are producing 95 million m^3/day of desalinated water. Almost half of global desalination capacity (48%) is located in Middle East and North Africa[3]. Development of membrane-based desalination is gradually replacing thermal based desalination. By 2000, the membrane-based desalination was producing 50% of the desalinated water. Now a days, membrane desalination is producing 65.5 million m^3/day of the total 95 million m^3/day of desalinated water[3]. The membrane-based desalination is a leading technology to desalinate widely available sea water[4]. The success and significance of membrane desalination is evident from the fact that this technology has been in practice for the last 30 years[5].

Polyamide membranes have been extensively studied and applied at commercial scale for multivariate applications such as nanofiltration, wastewater treatment, organic solvent nanofiltration, chiral separations and reverse osmosis[5,6]. These membranes are designed to have a fine pore structure with highly selective polyamide layer[7]. A uniformly distributed fine pore structure of the membrane enables the separation of Angstrom sized molecules. A lot of progress has been made by researchers in improving the capability of polyamide membranes regarding nanofiltration (NF) and reverse osmosis (RO)[8].

Thin film composite nanofiltration membranes (TFC-NF) are widely used in industrial and commercial scale setups. Generally, NF membranes possess an architecture of having thin film composite structure with polyamide active layer. The fabrication of membrane is carried out through interfacial polymerization (IP) where an aqueous solution of an amine is reacted to an acid chloride contained in a non-aqueous (n-hexane) phase[9,10]. The amines that are most commonly employed in IP are diamines such as piperazine (PIP), m-phenylenediamine (MPD), ethylenediamine (EDA), which are commonly cross-linked by reacting with trimesoyl chloride (TMC). The diamine and TMC react through Schotten-Baumann reaction leading to hyper-cross-linked polyamide active layer[11]. Although, a lot of progress has been made in this dimension but most of the work has been limited to diamines, which offer just two reaction sites for cross-linking and hence limit the degree of cross-linking. However, the availability of a multitude of amines with three or four active amine functions and readily hexane-soluble cross-linkers such as terephthaloyl chloride (TPC) allow further tunability of the pore structure and thickness of the polyamide active layer leading to fabrication of

[1]Interdisciplinary Research Center for Membranes and Water Security, King Fahd University of Petroleum and Minerals, Dhahran 31261, Saudi Arabia.
✉email: abdul.waheed@kfupm.edu.sa

thin, selective, and highly cross-linked polyamide network. In a work carried out by Lee et al.[12], various amines including MPD, EDA, PIP, diethylene triamine (DETA), Melamine, and tetraethylene pentaamine (TEPA) have been cross-linked by using cyanuric chloride (CC) as a cross-linker. Out of all the fabricated membranes in this work, the DETA/CC membrane was the best membrane in terms of flux (15.0 LMH) and salt rejection (85.2% of NaCl)[12]. Similarly, in another work a relatively less explored and readily hexane-soluble cross-linker terephthaloyl chloride (TPC) has been employed to fabricate a nanofiltration membrane for organic solvent nanofiltration (OSN) and the fabricated membrane was able to reject most of the tested dyes such as Nile red and Rhodamine while the structure of the membrane remained intact in different organic solvents such as methanol and ethanol[6]. Trivedi et al.[13] has synthesized a polyamide TFC-NF membrane by using polyethyleneimine (PEI) and TMC with a molecular weight cut off (MWCO) of ≈180 Da with a permeate flux of 14–24 L m^{-2} h^{-1} bar^{-1} [13]. Similarly, multifunctional linear amines such as DETA has also been used in fabrication of interlayer during membrane preparation. It has been found that an interlayer prepared by constituting DETA and tannic acid lead to a TFC-NF membrane with >98% rejection of Na_2SO_4[14]. Hence, exploration of the potential of multifunctional amines for synthesizing highly selective polyamide active layers, leading to promising TFC nanofiltration membranes is an area that needs attention by the research community. Therefore, in this work an IP reaction has been carried out by selecting a set of two linear monomers namely N,N-bis(2-aminoethyl)-1,3-propanediamine **1**, a tetramine, and TPC **2** (Supplementary Fig. 1). The amine **1** possesses four amine functions including two primary (-NH_2) and two secondary (-NH) amines in a single molecule, which provides four reactive sites for cross-linking. The reaction of amine **1** allows a knitting type of reaction with TPC **2** yielding a highly dense and selective polyamide network on PS/PET membrane support. Both monomers namely N,N-bis(2-aminoethyl)−1,3-propanediamine **1** and TPC **2** selected for current study have lower cost compared to commonly used amines (PIP and MPD) and cross-linker (TMC), which could potentially reduce the overall cost of polyamide TFC nanofiltration membrane fabrication. Moreover, the linear structure of the TPC makes TPC an ideal cross-linker with minimum stearic hindrance, which makes the cross-linking more feasible and extensive.

Keeping in view the significance and efficient utilization of the multiple amine functions in a single molecule during IP, we decided to fabricate a membrane by using multifunctional amine instead of conventional diamines. Instead of using conventional monomers, we have used N,N-bis(2-aminoethyl)-1,3-propanediamine **1** as a tetra-amine possessing four amine functions per molecule. The tetra-amine was efficiently reacted with TPC **2** used as a cost effective and efficient cross-linker with acid chloride present at para-positions. The **IP** between two low cost, simple and highly reactive monomers namely amine **1** and TPC **2** has resulted in the fabrication of a hyper-cross-linked and dense polyamide thin film composite nanofiltration (HCPA-TFC-NF) membranes. As the fabricated membrane HCPA-TFC-NF possessed a unique polyamide network, we decided to tune the structure of the HCPA-TFC-NF membrane and hence various factors such as effect of curing temperature and duration of curing was studied in depth to find the best performing version of HCPA-TFC-NF membrane. The fabricated membranes were tested for their nanofiltration efficiency in terms of selectivity and flux over cross-flow filtration setup. The fabricated membranes efficiently removed the divalent ions from the feed solutions. Moreover, the effect of hydrofluoric acid (HF) treatment on the membrane stability and performance efficiency has also been evaluated.

RESULTS AND DISCUSSION

Evaluation of chemical structure of the membranes using FT-IR and Solid ^{13}C NMR analysis

In order to further establish the structure and confirm the cross-linking success of the monomers **1** and **2** through IP, cross-polarization magic angle spinning (CP-MAS) experiments were performed to determine the solid ^{13}C NMR of the polyamide active layer. In order to avoid the interference of the support layers, the polyamide active layer was fabricated in vial as shown in Fig. 1a. The peaks at 175.82 ppm indicate the carbonyl >C=O function of amide while the peak at 133.20 ppm is attributed to the aromatic carbons of TPC **2** while the peaks at 48.64 and 40.93 ppm are due to the aliphatic carbons of the amine **1** (Fig. 1b). All of these peaks confirmed the successful cross-linking and establishing of hyper-cross-linked polyamide active layer of HCPA-TFC-NF membrane as indicated in the proposed structure of the active layer in Fig. 1c.

The presence of various functionalities in the active layer was confirmed by ATR-FTIR (Fig. 1d, e). The most important function is the amide linkage (-CONH-), which confirms the success of the reaction between amine **1** and acid chloride (TPC, **2**), leading to the formation of polyamide active layer. It is evident from the FTIR spectrum of TPC that the peak at 3000 cm^{-1} is indicative of =C–H bond of the aromatic ring of the TPC while a strong peak at 1723 cm^{-1} is representative of the carbonyl (>C=O) moiety of the acid chloride function. In case of amine **1**, the distinguishing peaks are a broad peak at 3292 cm^{-1} and a narrow peak at 2919 cm^{-1}, which are attributed to the -N–H and aliphatic -C–H functions present in the amine structure as shown in Fig. 3a. Most importantly, the FTIR spectrum of the hyper-cross-linked polyamide active layer possesses all of the characteristics peaks of the reacting amine **1** and TPC **2**. A broad and strong peak in a region of 3600–3400 cm^{-1} (Fig. 3b) is attributed to the presence of amide -N–H bond. The peaks at 3000 cm^{-1} to 2900 cm^{-1} are due to the =C–H and -C–H, which are attributed to aromatic functions and aliphatic chains present in the structure of the polyamide network. Furthermore, another characteristic narrow and strong peak is located at 1620 cm^{-1} (Fig. 3c), which is due to the presence of carbonyl (>C=O) of amide linkage in active layer. The presence of all these peaks that are mentioned above affirms the success of IP, leading to the formation of hyper-cross-linked polyamide active layer. A detailed account of all the characteristic peaks is given in the Supplementary Table 1.

The ATR-FTIR spectra of the PET support, PSf support and the HCPA-TFC-NF@M1, HCPA-TFC-NF@M2 and HCPA-TFC-NF@M3 membranes are shown in the Fig. 2a, b. It is visible that the PET (Supplementary Fig. 1) lacks any peak in the amide -N–H region of 3600 cm^{-1} to 3400 cm^{-1} while a characteristic peak at 1600 cm^{-1} is present in case of PET due to ester linkage (Supplementary Fig. 2). Similarly, the PS/PET ATR-FTIR also lacks the peaks characteristics of polyamide. However, the fabricated membranes show a broad band in the range of 3600–3400 cm^{-1} attributed to the amide -N–H linkage while the >C=O frequency of amide bond is overlapped with >C=O of the PET support. Hence, the interpretation of FTIR of the support and TFC membranes shows that an active polyamide layer has been successfully grown on the support leading to HCPA-TFC-NF membranes. However, intensity of the peaks of hyper-cross-linked polyamide active layer is relatively lower that can be attributed to the presence of a very thin nm scale active layer, which may not be enough for the FTIR to show with a significant profile. Keeping this fact in mind the FTIR spectrum of the free-standing active layer was recorded where all of the required peaks are clearly evident as shown in Fig. 1d.

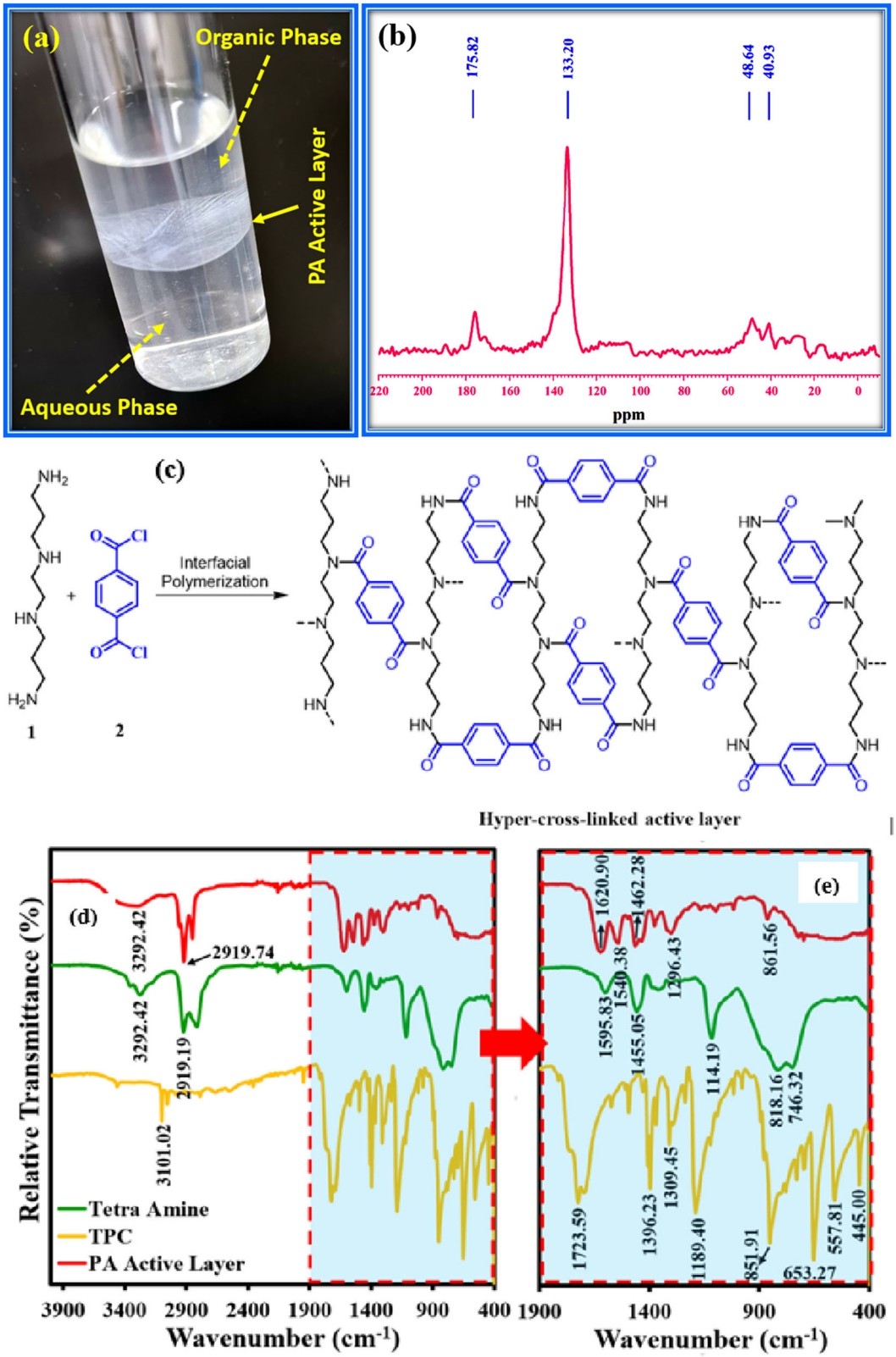

Fig. 1 Free-standing active layer, solid NMR, and FTIR analysis of active layer and reacting components. a A free-standing active layer as white sheet at the interface between the two phases, **b** and the solid (CP-MAS) ^{13}C NMR of the active layer generated by reacting amine **1** and TPC **2**. **c** The reaction conditions and the proposed structure of the hyper-cross-linked polyamide active layer. **d** The FTIR of amine **1**, TPC **2** and polyamide active layer showing the region from 4000 cm^{-1} to 400 cm^{-1} while **e** the peaks of carbonyl along with fingerprint region.

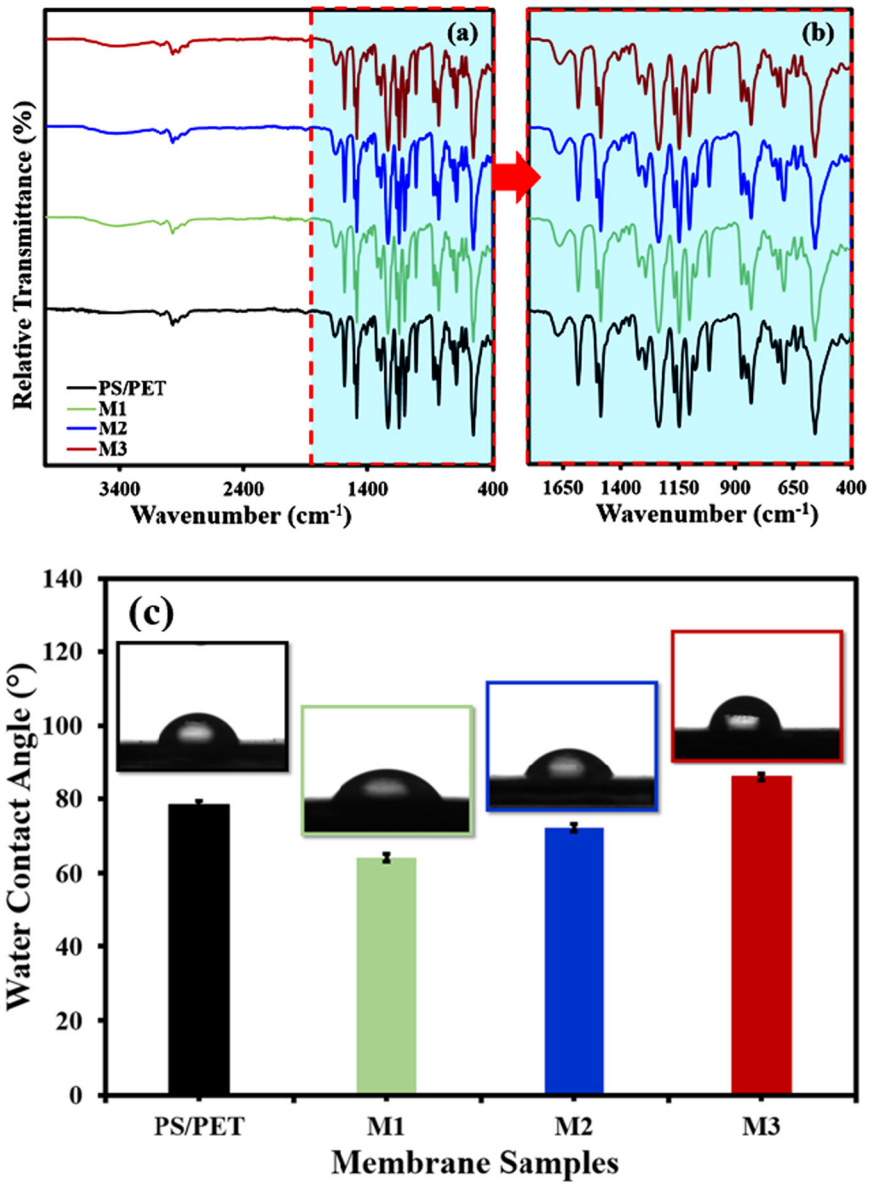

Fig. 2 ATR-FTIR and water contact angle of membranes. a, **b** FTIR of the support (PS/PET) and TFC-NF membranes**:** HCPA-TFC-NF@M1, HCPA-TFC-NF@M2, and HCPA-TFC-NF@M3. **c** Variation of water contact angle of support and the membranes HCPA-TFC-NF@M, HCPA-TFC-NF@M2, and HCPA-TFC-NF@M3.

Surface features of the membranes

The surface wettability of the membranes was measured through WCA measurements. The WCA of the PS/PET support was decreased upon introduction of polyamide active layer on the support that is attributed to the presence of free amine functions and partially due to the carboxylic functions, which are generated due to hydrolysis of the acid chloride moieties of the TPC[15]. Moreover, the water contact angle showed following increasing trend HCPA-TFC-NF@M1 < HCPA-TFC-NF@M2 < HCPA-TFC-NF@M3 with contact angle of 64.2°, 72.2°, and 85.9° (Fig. 2c). This can be attributed to an increased degree of cross-linking at higher temperatures, leading to complete cross-linking of TPC with free amine functions. An extensive cross-linking of TPC leads to a decrease in number of residual -COCl functions to be hydrolyzed into -COOH, a hydrophilic group. These observations are also reflected in the pattern of flux followed by the membranes. In the current study, a higher water flux (50 L m^{-2} h^{-1} at 20 bar) was shown by HCPA-TFC-NF@M1 as it has the lowest WCA while lowest water flux (25.71 L m^{-2} h^{-1} at 20 bar) was found in case of HCPA-TFC-NF@M3 as it has the higher WCA value. This observation is generally accepted where the decrease in WCA leads to an increased hydrophilicity and higher flux of the membranes[16].

Morphological and elemental characteristics of the membranes

FE-SEM was performed to reveal the morphological features of the membranes (Fig. 3). The surface morphology of the HCPA-TFC-NF@M2 membranes can be seen in Fig. 3d–f where it is visible that the PSf support is completely covered by polyamide active layer, which shows that IP was not limited to surface instead the porous nature of the support membrane has allowed amine **1** to diffuse deeper and the polymerization has been taking place continuously from within the pores of the ultrafiltration PSf support, leading to formation of a continuous polyamide active layer, which has resulted into a highly selective membrane. The surface

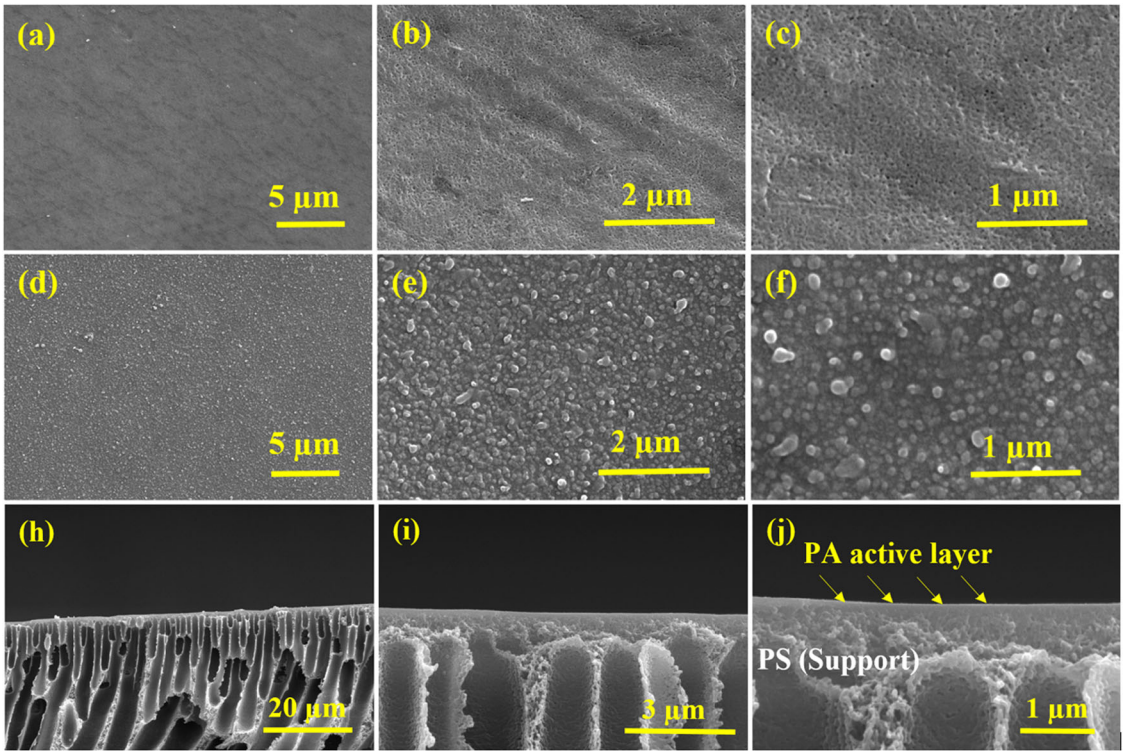

Fig. 3 Morphological analysis of membranes. FE-SEM images of the PS/PET support (**a**–**c**) and HCPA-TFC-NF@M2 (**d**–**f**) membranes at three different magnifications, **h**–**j** cross-sectional images of HCPA-TFC-NF@M2 at different magnifications.

morphology is showing a structure different from the traditional ridge and valley morphology of the MPD/TMC membrane.

To see the uniformity and intactness of PS/PET and HCPA-TFC-NF@M2, different magnifications of the support and HCPA-TFC-NF@M2 micrographs are shown in Fig. 3. The Fig. 3a–c shows that the porosity of the membrane becomes visible as the magnification reaches to 1 µm (120KX). It can be seen that the pores are uniformly distributed in the support with smooth surface features. However, the micrographs (Fig. 3d–f) of the HCPA-TFC-NF@M2 are showing that the pores of support are progressively covered by an active layer, leading to the formation of a continuous hyper-cross-linked polyamide active layer on the support. Moreover, the globular appearance of the active layer (Fig. 3f) is also a confirmation of the extensive cross-linking, leading to polyamide network leading to membrane. Cross-sectional micrographs of the membranes were also shown in Fig. 3h–j. The cross-sections of the membrane revealed the formation of a highly dense skin layer of polyamide on the top followed by highly porous support. The presence of finger-like projections in the ultrafiltration support provided the channels for transport of permeate through the membrane.

The structure of the membrane active layer is dependent upon the kinetics and mechanism of IP. The TPC is highly reactive bifunctional cross-linker, which possesses acid chloride on para-positions of the benzene ring. As TMC is analogous in structure to TPC with the exception of a third acid chloride but TMC is violently reactive at room temperature, leading to the formation of a hyper-cross-linked polyamide active layer in conventional MPD or PIP/TMC membrane. Hence, the TPC being more soluble in hexane than TMC and possessing acid chloride groups at para-positions make the diffusion and reaction of the TPC faster, leading to the formation of a hyper-cross-linked polyamide network with multi-functional amine **1**. Amine **1** being aliphatic in nature possesses a continuous chain like structure with equal ratio of primary (two -NH_2) and secondary amine (two -NH) groups, which fulfils the requirement of hyper-cross-linking where at least one of the reacting monomers must be trifunctional as amine **1** is tetrafunctional. These features of TPC **2** and amine **1** make these monomers ideal for fabricating a highly selective hyper-cross-linked polyamide active layer with a flux of 35.71 L m^{-2} h^{-1} and rejection of 87.36% for NaCl by HCPA-TFC-NF@M2 membrane at 20 bar.

Energy dispersive spectroscopy (EDS) results (Supplementary Fig. 3) of the HCPA-TFC-NF@M2 membrane have revealed the presence of all of the essential elements including Nitrogen (N), Carbon (C), Oxygen (O), and Sulfur (S), which are believed to be originating from polyamide active layer and PS/PET support. As active layer is composed of polyamide that possesses -CONH- linkages while S is a component of PSf support, and the remaining elements are commonly found in all of the layers of TFC membrane. The N is present in case of HCPA-TFC-NF@M2 while N is absent in case of PS/PET that is due to the formation of polyamide, which is not present in case of PS/PET support. However, a lower percentage of N suggests that active layer is comparatively narrower than the support PS/PET membranes. These findings confirmed the success of membrane fabrication and integrity of TFC membranes. Moreover, after the deposition of active layer, the percentage of C and S is decreased while that of O is increased which indicates that the thickness of the membrane has increased, which is in agreement with the previous studies in literature[15,17].

Elemental mapping results of the HCPA-TFC-NF@M2 is shown in Fig. 4, where it is clearly evident that the support is composed of the elements namely C, O and S. The mapping results show that all of the elements are equally distributed in PS/PET support while in case of HCPA-TFC-NF@M2 all of the elements including C, O, and S are present with equal distribution with an additional and equally distributed N element, which is due to amide bond of active layer[18].

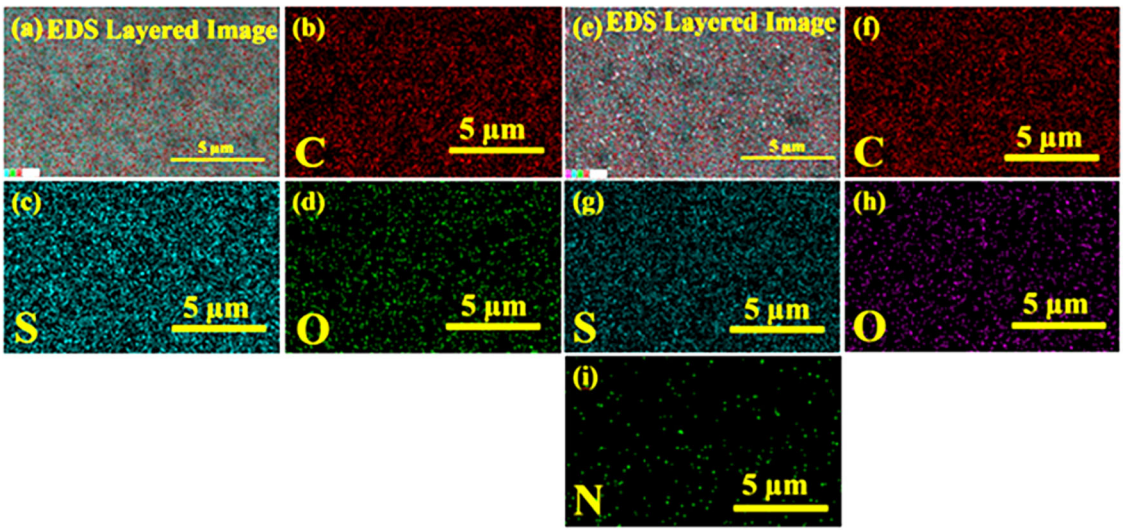

Fig. 4 Elemental analysis of the membranes. a–d Elemental mapping analysis of the PS/PET support for the Carbon (C), Sulfur (S), and Oxygen (O) and **e–i** Elemental mapping analysis of the HCPA-TFC-NF@M2 membrane for the Carbon (C), Sulfur (S), Oxygen (O), and Nitrogen (N).

To get a further insight into the surface features of fabricated membranes, AFM measurement was carried as shown in the following Fig. 5. The surface roughness of the bare PS/PET membrane (Fig. 5a, b) showed a relatively smoother surface compared to that of the HCPA-TFC-NF@M2 membrane (Fig. 5c, d). An increase in surface roughness after the deposition of polyamide active layer is an indication of formation of an active layer over the PS/PET support. The surface average roughness was increased from $R_a = 7.65$ nm (PS/PET) to $R_a = 10.2$ nm (HCPA-TFC-NF@M2) after the deposition of polyamide active layer.

The surface composition of the membranes was investigated as shown in Fig. 5e. An XPS analysis of PS/PET support indicated the presence of constituent elements such as Carbon (C1s), Oxygen (O1s), and Sulfur (S2p), which are attributed to the PS/PET support. In case of HCPA-TFC-NF@M2 membrane, an additional element Nitrogen (N1s) was also found along with C1s, O1s and S2p. The presence of N1s indicated the presence of polyamide network on the ultrafiltration support. Another important observation was the suppression of the S1s peak, which might be attributed to the covering of the PS/PET support. All these characterizations confirmed the successful formation of the polyamide active layer on PS/PET ultrafiltration support.

The high-resolution XPS spectra of the PS/PET support and the HCPA-TFC-NF@M2 membranes are given in the following Fig. 5 (f–l). The deconvolution of the survey scan of PS/PET possesses two carbon peaks at 284.5 eV and 286.6 eV, which might be attributed to the C–C and C–S bonds of PSf (Fig. 5f). However, O1s showed only single peak at 530.5 eV, which can be attributed to the S=O bond of PSf (Fig. 5g). The deconvolution of the S2p peak showed the two peaks located at 163.2 eV and 168.1 eV due to S=C and S=O bonds of PSf (Fig. 5h). However, after the formation of polyamide active layer, the carbon peak was splitted into three peaks located at 283.8 eV, 285.5 eV and 286.3 eV, which might be attributed to C–C, C–N, and C=C bonds (Fig. 5i). Quite interestingly, the O1s peak was splitted into two distinct peaks at 529.5 eV and 531.5 eV, which were attributed to carbonyl (C=O) bond of primary and secondary amide (-CONH) linkages of active layer (Fig. 5j). The similar two S2p peaks were seen with highly reduced intensity, which indicated that the PS/PET support was fully covered by polyamide active layer (Fig. 5k). The deconvolution of N1s peak showed the presence of a single peak located at 398.4 eV, which confirmed the successful formation of polyamide active layer (Fig. 5l).

The surface zeta-potential of the membranes was measured as given in Supplementary Fig. 4. It was found that at acidic pH, the HF-treated HCPA-TFC-NF@M2 was more positive than untreated HCPA-TFC-NF@M2. The HF-treated HCPA-TFC-NF@M2 showed negative charge at highly basic pH = 10.3 while untreated HCPA-TFC-NF@M2 showed negative charge at pH = 6.4. The isoelectric point for HF-treated membrane lies at ≈pH = 8.3 while for untreated HCPA-TFC-NF@M2, it lies at ≈pH = 6.0. This trend can be attributed to an excessive protonation of HCPA-TFC-NF@M2 due to acidic protons of HF and deprotonation of HF-treated HCPA-TFC-NF@M2 needs stronger basic conditions. Owing to the need of strong basic conditions for deprotonation, the HF-treated HCPA-TFC-NF@M2 showed a negative charge at pH > 8.2. Moreover, the negative charge of HF-treated HCPA-TFC-NF@M2 is also more than the untreated HCPA-TFC-NF@M2.

Effect of curing temperature on the degree of cross-linking in polyamide active layer

To find out the best conditions for fabrication of a suitable membrane with reasonable flux and higher selectivity and with an idea of dependence of cross-linking on temperature, the study of the effect of different curing temperatures was conducted. The study was carried out by setting the curing temperature at three different values including 60, 80, and 100 °C for a period of 30 minutes as depicted in the Fig. 6a and the membranes were named as HCPA-TFC-NF@60, HCPA-TFC-NF@80 and HCPA-TFC-NF@100, respectively. It is evident from Fig. 6a that an increase in curing temperature led to decrease in the flux of water, which can be attributed to increased cross-linking and dense polyamide active layer with the increasing temperature. Among all of the tested membranes, the highest flux was achieved in case of HCPA-TFC-NF@60 reaching to 68.57 L m^{-2} h^{-1} while the lowest flux was observed in case of curing temperature of HCPA-TFC-NF@100 with a value of 18.57 L m^{-2} h^{-1} while a moderate value of flux (41.71 L m^{-2} h^{-1}) was achieved in case of HCPA-TFC-NF@80.

The rejection of the salts such as $CaCl_2$, $MgCl_2$, and Na_2SO_4 was studied at a feed concentration of 2 g L^{-1}. The conductivity and total dissolved solids (TDS) of both feed and permeate were measured and % rejection of salts (Fig. 6b) was measured based on TDS values by using Eq. 2. The highest salt rejection was attained in case of 100 °C as a curing temperature while the lowest rejection was observed in case 60 °C of curing temperature. All of

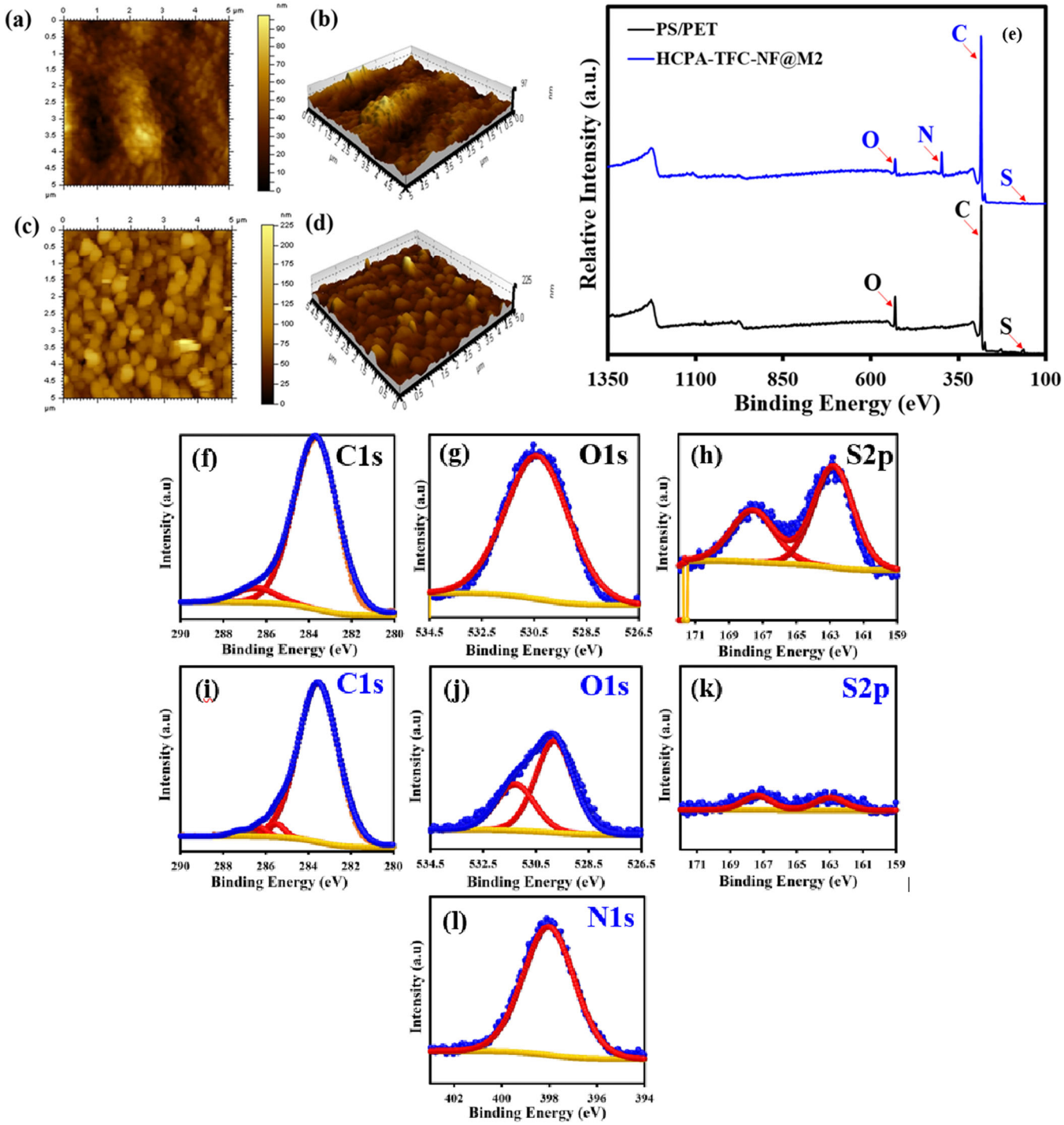

Fig. 5 AFM and XPS analysis of membranes. a, **b** 2D and 3D AFM images of the PS/PET support and **c**, **d** HCPA-TFC-NF@M2 membranes and **e** XPS survey scans of the PS/PET support and HCPA-TFC-NF@M2 membranes. The deconvolution of XPS survey scans of the **f**–**h** PS/PET support and **i**–**l** HCPA-TFC-NF@M2 membranes.

the fabricated membranes showed highest rejection for $MgCl_2$ as it is evident from Fig. 6b.

Effect of curing time on the degree of cross-linking in polyamide active layer

Based on the performance of the different membranes, the curing time was increased with an interval of 30 min each with values of 30, 60, and 90 min at a constant temperature of 80 °C and the membranes were named as HCPA-TFC-NF@0.5, HCPA-TFC-NF@1.0 and HCPA-TFC-NF@1.5, respectively (Fig. 6c). The flux was measured again at 20 bar, and it was observed that the highest flux (41.71 L m^{-2} h^{-1}) was achieved for membrane cured for HCPA-TFC-NF@0.5 while lowest value of flux (34.28 L m^{-2} h^{-1}) was obtained with a curing temperature of HCPA-TFC-NF@1.5. These observations suggest that active layer has been densely hyper-cross-linked leading to fine pores and resulting into reduced flux. However, the curing time of 60 min was found reasonable as the

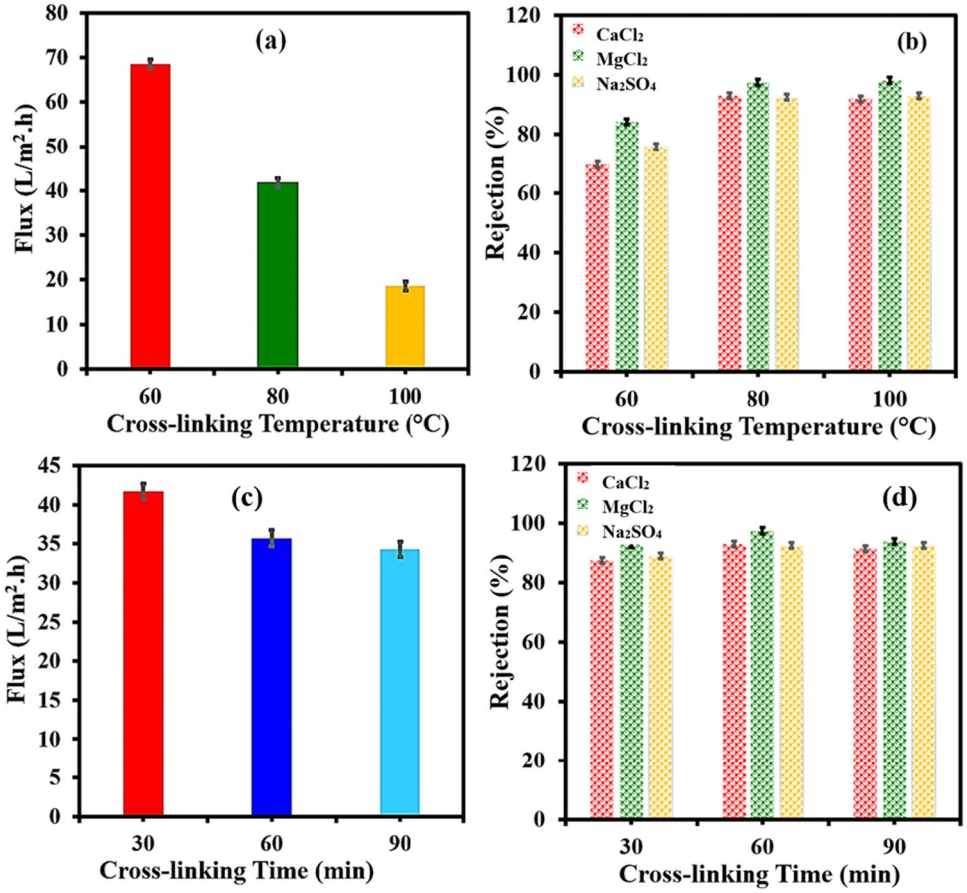

Fig. 6 Study of various factors on membrane performance. Effect of cross-linking temperature on **a** water flux and **b** salt rejection at constant pressure (20 Bar) and constant cross-linking time (30 min). **c** Effect of cross-linking time on water flux and **d** salt rejection at constant temperature (80 °C) and constant pressure (20 Bar).

flux was found to be excellent for the HCPA-TFC-NF@1.0 with a value of 35.71 L m^{-2} h^{-1}. A comparison of flux of all the membranes at different curing times is depicted in Fig. 6c. The % rejection of salt by all the membranes was also studied where the rejection of the tested salts stayed >85% for all the fabricated membrane with all of the tested salts while the rejection was higher in case of cross-linking time of 60 and 90 min of curing (Fig. 6d).

In pursuit of evaluation of the parameters for controlling degree of hyper-cross-linking leading to the fabrication of excellently performing membrane and keeping the effect of curing time and curing temperature in mind, we fabricated membranes namely HCPA-TFC-NF@M1, HCPA-TFC-NF@M2, and HCPA-TFC-NF@M3 as these membranes were fabricated at three different temperatures 60, 80, and 100 °C with a curing time of 60 min. The flux of all the tested membranes was measured at varied transmembrane pressures. It can be seen that the flux is linearly related to the applied transmembrane pressure as shown in Fig. 7a.

As anticipated, the highest salt rejection was observed in case of HCPA-TFC-NF@M3 while the lowest salt rejection was observed in case of HCPA-TFC-NF@M1 for all of the tested salts including NaCl (Fig. 7b). The highest salt rejection was observed in case of $MgCl_2$ reaching to a value of 98.11% in case of HCPA-TFC-NF@M3 and it was found to be 97.45% in case of HCPA-TFC-NF@M2 while the % rejection of $MgCl_2$ was reduced to 94.59% in case HCPA-TFC-NF@M1. These observations support the fact that as the degree of cross-linking increases, the membrane shows increased rejection. To find the best tradeoff agreement between the two rivals (flux and rejection), the best membrane was found to be HCPA-TFC-NF@M2, which was fabricated at 80 °C for 60 min (Fig. 7b).

A highly significant finding was rejection of NaCl. The % rejection of NaCl was found to be 87.36% and 93.28% in case of HCPA-TFC-NF@M2 and HCPA-TFC-NFM3, respectively (Fig. 7b). Moreover, the fabricated membranes can tolerate higher values of transmembrane pressure reaching up to 30 bar, which can again be attributed to the use of multiple amine sites available for cross-linking through TPC, leading to the formation of strong hyper-cross-linked network. These features of rejecting NaCl and keeping the membrane integrity even at higher transmembrane pressures make such hyper-cross-linked membranes reverse osmosis (RO) like NF membranes. The coefficient of solute permeability (B_{exp}) was also determined based on concentration polarization by using Supplementary equation 1 and 2, respectively[19], and the results are given in Supplementary Fig. 5. It was observed that solute permeability increases as the ions changes from divalent ions (Mg^{2+} and SO_4^{2-}) to monovalent ions (Na^{1+} and Cl^{-1}). $MgSO_4$ showed a lowest permeability (0.23 LMH) while NaCl was found to be the most permeable salt (5.8 LMH). The salts with a combination of monovalent and divalent ions (Na_2SO_4) showed a permeability of 3.5 (LMH; L m^{-2} h^{-1}). This might be attributed to higher values of TDS (total dissolved solid) of NaCl compared to other salts, which under high pressure gets concentrated near the membrane surface. Given the higher concentration of NaCl near membrane surface, it showed high permeability than other salts.

In order to explore the stability of the HCPA-TFC-NF@M2 membrane, long-term stability test was carried out where the membrane was able to maintain the rejection at a constant level. The flux was slightly decreased, which might be due to the

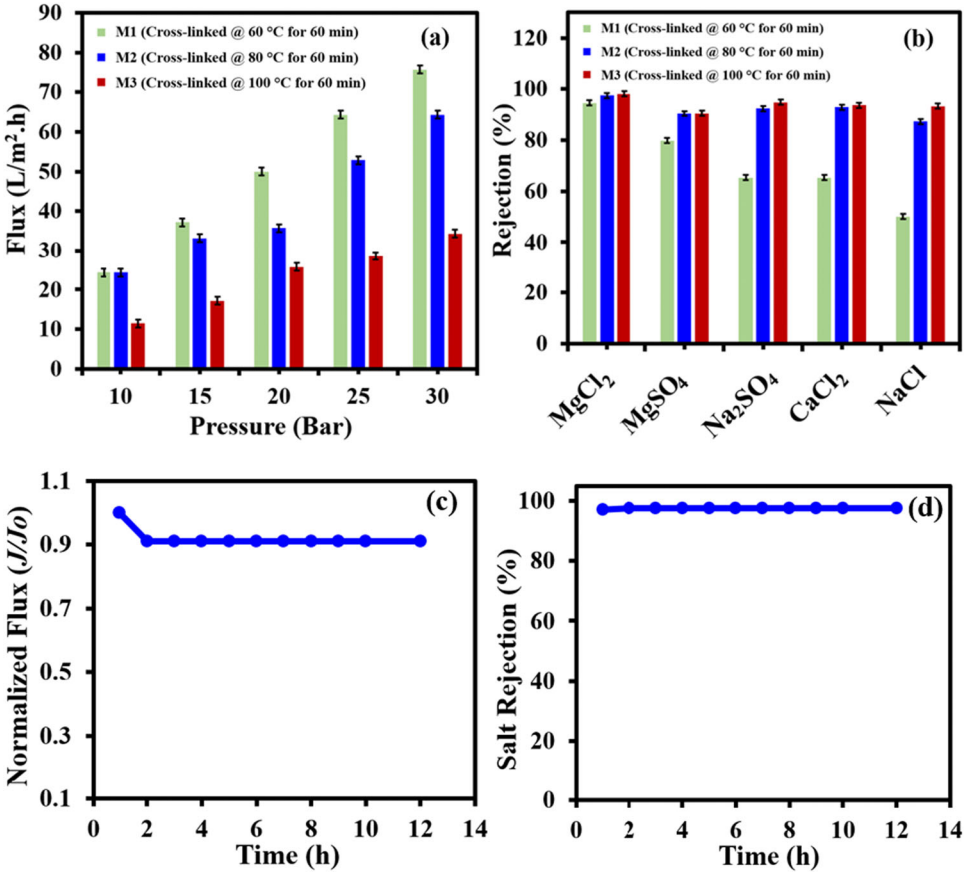

Fig. 7 Study of transmembrane pressure variation and salt rejection. a Effect of different pressure on water flux of the membranes, fabricated at different cross-linking temperature (Temperature: 60, 80, and 100 °C; Time: 60 min) using cross-flow nanofiltration setup, **b** Salt rejection performance of the membranes, fabricated at different cross-linking temperatures 60, 80, and 100 °C; Cross-linking Time: 60 min) using cross-flow filtration setup at constant pressure (20 bar) and **c**, **d** long-term stability test for performance evaluation of HCPA-TFC-NF@M2.

deposition of some rust from stainless steel filtration setup on the membrane surface (Fig. 7c, d).

The effect of hydrofluoric acid (HF) treatment on performance of HCPA-TFC-NF@M2

The HCPA-TFC-NF@M2 membrane was treated with 15% solution (v/v) of HF by simple immersion method. Compared to literature where the polyamide membranes have been exposed to lower concentration of HF such as 1% aqueous HF for certain period of time[20], HCPA-TFC-NF@M2 has been kept in 15% aqueous HF solution for a period of 120 h of immersion of membrane in the HF solution allowing considerable reaction time. The HCPA-TFC-NF@M2 membrane was found to be visibly intact. As the polyamide active layer has been fabricated by using a multi-function amine and TPC, there is a possibility of availability of unreacted amine function in the hyper-cross-linked polyamide network. The HF was added with the idea of protonation of the unreacted amine functions leading to the formation of ammonium ions in the polyamide network with fluoride as a counter anion as depicted in the proposed structure of the active layer after HF treatment in Fig. 8a. The generation of ammonium ion function in the polyamide active layer leads to higher hydrophilicity without destroying the pore structure of the membrane, which results into higher flux compared to untreated membrane. It can be seen that the flux was increased by 1.75 folds in case of HF-treated HCPA-TFC-NF@M2 than untreated version of HCPA-TFC-NF@M2 with flux jumping from 35.71 L m^{-2} h^{-1} to 80 L m^{-2} h^{-1} (Fig. 8b). The % rejection was also maintained with a minor decrease even after the treatment with HF, which indicates that the pore structure of the membrane has been intact even after HF treatment (Fig. 8c).

To validate our assumption of increase in hydrophilicity of the membrane after treatment with HF, we characterized the membrane for its hydrophilicity by measuring its WCA, which was considerably decreased from 72.22° to 52.29° (Fig. 8d). This decrease in WCA of the membrane after treatment with HF supports observation of the higher flux of the membrane. Furthermore, the ATR-FTIR of the HF-treated membrane showed that the -N–H peak in the region of 3500 cm^{-1} became stronger and broader than that of the untreated membrane, which can be attributed to the protonation of the free -N–H function as depicted in Fig. 8e[21]. In order to further explore the intactness of the HCPA-TFC-NF@M2 after exposure to HF, AFM and SEM analysis before and after exposure to HF was also conducted. Both 2D and 3D AFM images of HCPA-TFC-NF@M2 before (Fig. 8f, g) and after (Fig. 8h, i) HF treatment showed an intact membrane structure. Similarly, SEM analysis also revealed that the HCPA-TFC-NF@M2 membrane retained its integrity after HF treatment (Fig. 8j–m).

The integrity of the fabricated membrane HCPA-TFC-NF@M2 was explored by measuring the flux of the membrane at varied feed temperatures. The flux was found to increase with the increasing feed temperature (Supplementary Fig. 6), which might be attributed to the increased mobility of the polyamide network chains allowing the easy diffusion of the water molecules through the membrane[22,23]. Moreover, an increase in feed temperature also causes a decrease in viscosity of solution leading to an

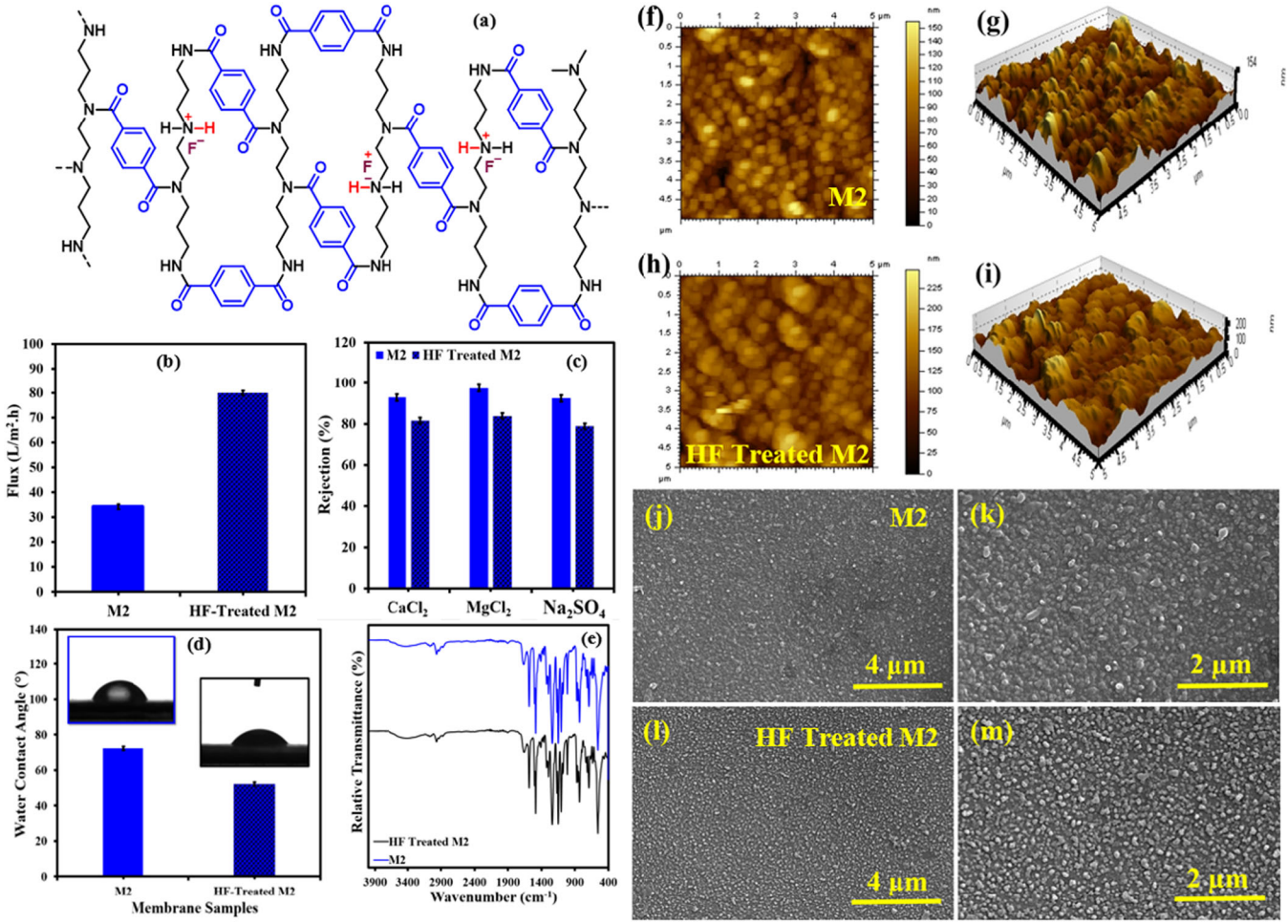

Fig. 8 Proposed structure and comparative characterization of HF-treated membrane. a The proposed structure of the protonated membrane active layer, **b** Performance of HCPA-TFC-NF@M2 membrane before and after treatment with HF in terms of pure water flux (**c**) and three different divalent ions rejection using cross-flow filtration setup at constant pressure (20 bar) and temperature (23 °C), **d** Water contact angle of HCPA-TFC-NF@M2 (M2) and HF-Treated HCPA-TFC-NF@M2 (HF-Treated M2) membranes and **e** FT-IR spectra of HCPA-TFC-NF@M2 (M2) and HF-Treated HCPA-TFC-NF@M2 (HF-Treated M2) membranes, **f**, **g** AFM images of HCPA-TFC-NF@M2, **h**, **i** AFM images of HF-treated HCPA-TFC-NF@M2, and **j**, **k** FE-SEM micrographs of HCPA-TFC-NF@M2 while (**l**, **m**) HF-treated HCPA-TFC-NF@M2.

increase in mobility of water molecules through membrane channels[7].

Removal of organic pollutant from the feed

After success with the removal of salts from feed solution, the membranes were applied for removal Eriochrome Black T (EBT) as a model organic pollutant from feed solution (Supplementary Fig. 7). Both of the membranes M2 and HF-treated M2 rejected >99% of EBT from the feed while the permeate flux was retained as in previous experiments. The permeate flux was found to be more than double for HF-treated membrane compared to untreated M2, which indicated that HF-treated M2 can be a candidate for treating a feed polluted with organic pollutants. A comparison of the performance of the membrane M2 with other similar membranes from literature is given in Table 1.

In summary, a set of HCPA-TFC-NF membranes was prepared by using multifunctional aliphatic amine possessing two primary and two secondary amine reaction sites in a single molecule and terephthaloyl chloride as a linear cross-linker. The choice of these unique monomers lead to successful fabrication of NF membranes with promising salt rejection and flux. The influence of curing temperature and curing time was also studied where 80 °C and 60 min were found to be the best curing temperature and curing time for membrane fabrication. The resulting membrane HCPA-TFC-NF@M2 showed a rejection for $MgCl_2$ and NaCl reaching to 97.45% and 87.36%, respectively, with water flux of 35.71 L m^{-2} h^{-1}. The HCPA-TFC-NF@M2 showed a rejection of >99% for EBT. Moreover, these membranes can tolerate relatively higher transmembrane pressure without losing performance in terms of rejection and flux, which makes these membranes an excellent chioce for treating the feed before passing it reverse osmosis membranes. The HF treatment enhanced the nanofiltration performance of the membrane. The long-term stability test revealed that salt rejection by HCPA-TFC-NF@M2 membrane stayed almost constant during filtration experiments for 12 h.

MATERIALS AND METHODS

Materials

N,N-bis(2-aminoethyl)−1,3-propanediamine **1** (97%), terephthaloyl chloride (TPC) **2** (99%), NaCl (99%), Na_2SO_4 (99%), $MgCl_2$ (98%), $CaCl_2$ (97%), $MgSO_4$ (99%), n-Hexane (95%), Triethylamine (TEA; 99%), polysulfone (PSf; 99%), dimethyl acetamide (DMAc; 99%), NaOH (98%), Hydrofluoric (HF; 48%) acid, sodium dodecyl sulfate (SDS, 98.5%) and Eriochrome Black T were purchased from Sigma Aldrich and polyetherterephthalate (PET) supports were used as it is without any further purification.

Table 1. The comparison of the HCPA-TFC-NF@M2 with membranes from literature.

Membranes	Chemicals used for interfacial polymerization	Water flux (L m^{-2}.h)	Rejection of divalent ions (%)	Rejection of monovalent ions (%)	Refs.
Polyamide/PES	1,3-phenylenediamine and Trimesoyl chloride	~24	~85%	~64%	[25]
Polyamide/PSf	Trimesoyl chloride and Piperazine	23.7	~95%	~40%	[26]
Polyamine/PSf	Polyvinylamine with Isophthaloyl chloride	4.15	~96.7%	~61.2%	[27]
Polyamide/PVDF	Trimesoyl chloride and Phenylenediamine	16	~96%	~68.14%	[28]
Polyamide/PES	Trimesoyl chloride and Piperazine	1.93	~95.1%	~35.5%	[29]
Polyamide/PSf	Trimesoyl chloride and Piperazine	~20	~95%	-	[30]
Modified polyamide/PEI	Trimesoyl chloride and Branched polyethyleneimine	~7	~85.4%	~81.5%	[31]
Polyamide/PSf	Trimesoyl chloride and Piperazine	~13.5	~91.1%	~35.7%	[32]
Polyamide/PSf	Cyanuric chloride and Piperazine	~1.06	~94.4%	~43.0%	[33]
Hyper-cross-linked polyamide/PSf	N,N-bis(2-aminoethyl)-1,3-propanediamine (Tetra-amine) and Terephthaloyl chloride	~35.71	~97.45%	~87.36%	This Work

Preparation of hyper-cross-linked polyamide HCPA-TFC-NF membranes

The membranes were fabricated by following the general procedure reported in literature[24]. The polysulfone support membranes were fabricated by phase inversion technique by using PET support. In order to increase wettability of polysulfone support, it was soaked in 0.05% sodium dodecylsulphate (SDS) aqueous solution for 24 h before the IP. For the fabrication of an active layer on PS/PET support, IP was carried out. In this typical procedure, the PS/PET supports were fixed on glass sheet and then an aqueous solution (2% w/v) of amine **1** (N, N′-bis(3-aminopropyl)ethylenediamine) containing certain volume of triethylamine (TEA) was poured onto the PS/PET support and it was impregnated for 10 min. The TEA was added as an HCl scavenger, which is generated during reaction of amine **1** and TPC **2**. After impregnation with amine **1**, excess amine was removed from the PS/PET support with the help of a rubber roller and the membrane was allowed to dry in air. Once the amine impregnated support was dried, n-hexane solution (0.15%) of cross-linker **2** (terephthaloyl chloride; TPC) was poured onto the membrane and the IP reaction was continued for 60 s, leading to formation of a hyper-cross-linked polyamide active layer resulting into the formation of HCPA-TFC-NF membrane. The excess cross-linker **2** was washed with n-hexane. The molecular structures of the reacting amine **1** and cross-linker **2** along with TEA are given in Supplementary Fig. 1 while the compositions of prepared solutions of amine **1** and cross-linker **2** (TPC) are as given in the Supplementary Table 2.

A free-standing active layer was also synthesized for the sake of characterization. For this purpose, solutions of amine **1** and TPC **2** were reacted in a vail and the obtained white solid at the interface between the two phases was collected and washed thoroughly with both water and n-hexane alternatively. The washed active layer was completely dried before analysis.

The various steps adopted during the fabrication of HCPA-TFC-NF membrane are given in Fig. 9.

Tailoring the pore structure of polyamide active layer by varying the curing temperature of membrane

The successful IP resulted into the formation of polyamide active (PA) layer on PS/PET support. The membranes were exposed to various temperatures such as 60, 80, and 100 °C in an air-drying oven to complete cross-linking.

Tailoring the pore structure of polyamide active layer by varying the curing time

The membranes were heated at different temperatures for different time intervals of 30, 60, and 90 min, respectively, and allowed to cool down to room temperature. Upon cooling, the obtained membranes were soaked into deionized water for 24 h before starting the filtration experiments. The composition of the amine **1** and TPC **2** solution are given in the Supplementary Table 2 along with the nomenclature of the fabricated membranes.

Tailoring the membrane structure and performance by hydrofluoric (HF) acid treatment

The best performing membrane HCPA-TFC-NF@M2 was treated with 15% HF aqueous solution (v/v) by simple immersion method[16] by soaking the membrane for 120 h and then the membranes were rinsed with DI water and tested again through cross-flow filtration setup.

Characterization of TFC-PA membranes

In order to ascertain the various functionalities originating due to cross-linking of the amine **1** and acid chloride **2**, Fourier Transform Infrared (FTIR, Nicolet iS50, Thermo Fisher Scientific) spectroscopy was performed. The ATR experiment was performed by scanning the membrane sheet in the ATR-FTIR instrument.

An active layer was fabricated by reacting solutions of amine **1** and TPC **2** in the presence of TEA as an acid acceptor and the solvents were discarded while the obtained white membranous solid was thoroughly washed with DI water and n-hexane for three times each to remove any of the unreacted monomers and the foam type active layer was heated in the oven at 80 °C for 1 h as this temperature was the best temperature for membrane fabrication. The obtained dried sample was loaded into the sample holder and solid ^{13}C NMR was recoded on a Bruker spectrometer (400 MHz, H-1 frequency) at a spinning rate of 8 kHz, CP (cross-polarization) contact time of 2 ms and delay time of 2 s.

The surface morphological features of HCPA-TFC-NF membranes were investigated by using Quatrro FE-SEM equipped with EDX analyzer (Thermo Fisher Scientific). The membrane samples were characterized after coating with gold. The hydrophilicity experiments were carried out by water contact angle (WCA) measuring using goniometer (CA-Drop Shape Analyzer DSA100E, KRUSS). A perfectly dried membrane was fixed on a glass slide and water droplet (2 µL) was created and dropped on the surface of the membrane and contact angle was measured. AFM was done on Agilent 5500 AFM while XPS analysis was carried out on VG

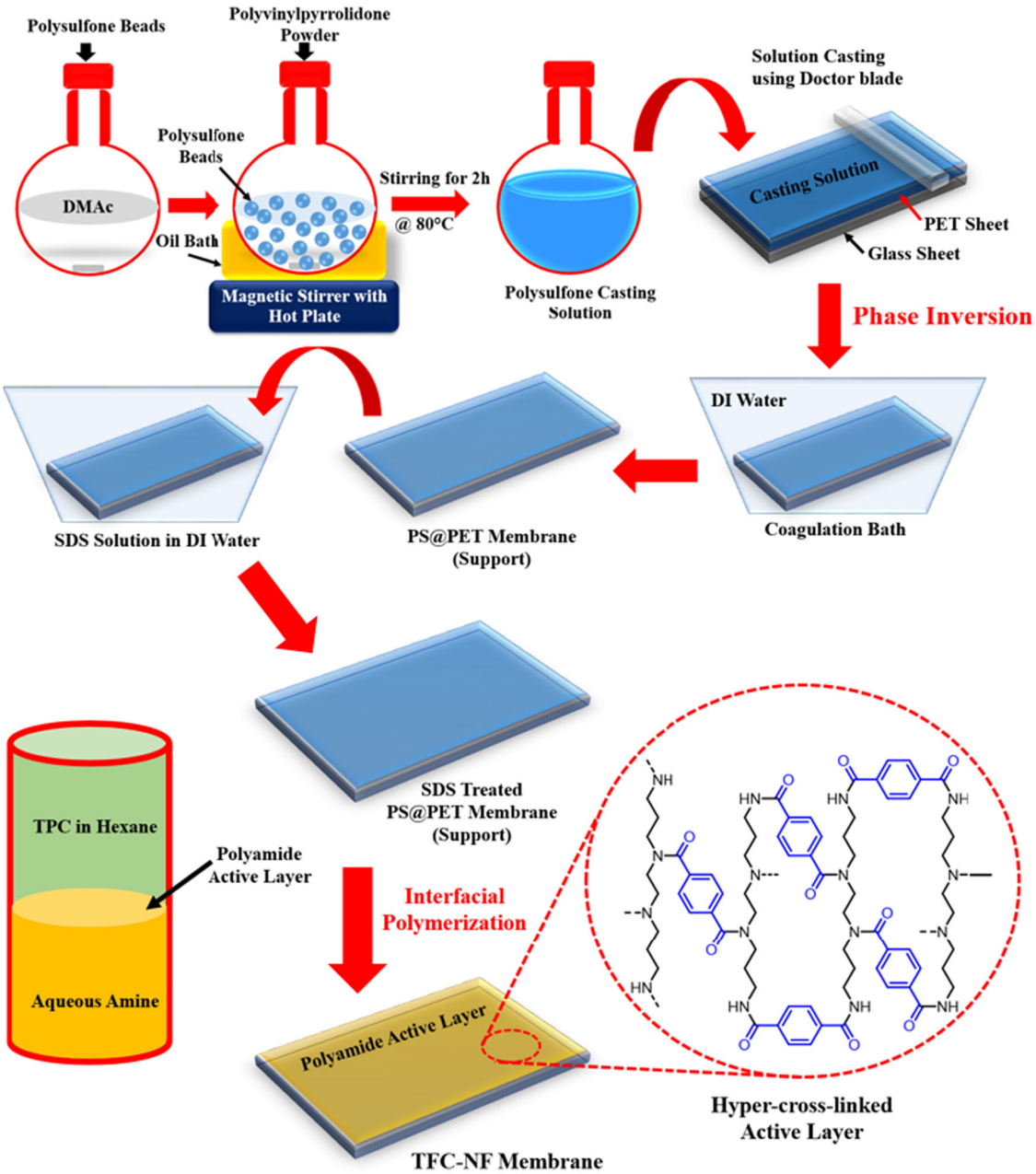

Fig. 9 Membrane fabrication scheme. Schematic diagram for the fabrication of hyper-cross-linked polyamide thin film composite nanofiltration (HCPA-TFC-NF) membranes.

Scientific ESCALAB MKII X-ray photoelectron spectrometer. The surface zeta-potential of the membranes was measured by Malvern Zetasizer Nano ZS at different pH values.

Nanofiltration evaluation of the membranes

The permeance and flux of the membranes were tested by cross-flow filtration experiments where DI water was used as feed. The flux is given by the following Eq. 1

$$J = \frac{V}{A \times t} \tag{1}$$

where J represents flux ($L\,m^{-2}\,h^{-1}$) of DI water, V represents the volume (L) of the permeate that has passed through the membrane, t is the time (h) taken by the permeate to pass through the membrane, A is the area (m^2) of the membrane. The rejection of the solutes was calculated by the following Eq. 2

$$R = \left(\frac{C_f - C_p}{C_f}\right) \times 100\% \tag{2}$$

where C_p is the concentration of the solute in the permeate and C_f is the concentration of the solute in the feed solution. The concentration of the solutes was kept at $2\,g\,L^{-1}$, which was measured by conductivity meter (Ultrameter II).

DATA AVAILABILITY

All data generated or analyzed during this study are included in this published article (and its supplementary information files).

Received: 30 November 2021; Accepted: 19 August 2022;
Published online: 21 September 2022

REFERENCES

1. Misra, A. K. Climate change and challenges of water and food security. *Int. J. Sustain. Built Environ.* **3**, 153–165 (2014).
2. Boretti, A. & Rosa, L. Reassessing the projections of the World Water Development Report. *NPJ Clean. Water* **2**, 1–6 (2019).
3. Jones, E., Qadir, M., van Vliet, M. T. H., Smakhtin, V. & Kang, S. M. U. The state of desalination and brine production: A global outlook. *Sci. Total Environ.* **657**, 1343–1356 (2019).
4. Hu, L., You, M. & Meng, J. Chlorination as a simple but effective method to improve the water/salt selectivity of polybenzimidazole for desalination membrane applications. *J. Memb. Sci.* **638**, 119745 (2021).
5. Ezugbe, E. O. & Rathilal, S. Membrane technologies in wastewater treatment: a review. *Membranes* **10**, 89 (2020).
6. Huang, T. et al. Molecularly-porous ultrathin membranes for highly selective organic solvent nanofiltration. *Nat. Commun.* **11**, 1–10 (2020).
7. Cheng, X. et al. Finely tailored pore structure of polyamide nanofiltration membranes for highly-efficient application in water treatment. *Chem. Eng. J.* **417**, 127976 (2021).
8. Yang, Z., Guo, H. & Tang, C. Y. The upper bound of thin-film composite (TFC) polyamide membranes for desalination. *J. Memb. Sci.* **590**, 117297 (2019).
9. Singh, R. Introduction to membrane technology. *Membr. Technol. Eng. Water Purif.* 1–80 https://doi.org/10.1016/B978-0-444-63362-0.00001-X (2015).
10. Zhang, L. et al. Polyamide nanofiltration membrane with high mono/divalent salt selectivity via pre-diffusion interfacial polymerization. *J. Memb. Sci.* **636**, 119478 (2021).
11. Akbari, A., Aliyarizadeh, E., Mojallali Rostami, S. M. & Homayoonfal, M. Novel sulfonated polyamide thin-film composite nanofiltration membranes with improved water flux and anti-fouling properties. *Desalination* **377**, 11–22 (2016).
12. Lee, K. P., Bargeman, G., de Rooij, R., Kemperman, A. J. B. & Benes, N. E. Interfacial polymerization of cyanuric chloride and monomeric amines: pH resistant thin film composite polyamine nanofiltration membranes. *J. Memb. Sci.* **523**, 487–496 (2017).
13. Trivedi, J. S., Bhalani, D. V., Bhadu, G. R. & Jewrajka, S. K. Multifunctional amines enable the formation of polyamide nanofilm composite ultrafiltration and nanofiltration membranes with modulated charge and performance. *J. Mater. Chem. A* **6**, 20242–20253 (2018).
14. Zhang, X., Lv, Y., Yang, H. C., Du, Y. & Xu, Z. K. Polyphenol coating as an interlayer for thin-film composite membranes with enhanced nanofiltration performance. *ACS Appl. Mater. Interfaces* **8**, 32512–32519 (2016).
15. Yang, Q., Xu, Z.-K., Dai, Z.-W., Wang, J.-L. & Ulbricht, M. Surface modification of polypropylene microporous membranes with a novel glycopolymer. *Chem. Mater.* **17**, 3050–3058 (2005).
16. González Muñoz, M. P. et al. Hydrofluoric acid treatment for improved performance of a nanofiltration membrane. *Desalination* **191**, 273–278 (2006).
17. Liu, S., Fang, F., Wu, J. & Zhang, K. The anti-biofouling properties of thin-film composite nanofiltration membranes grafted with biogenic silver nanoparticles. *Desalination* **375**, 121–128 (2015).
18. Lu, X. et al. Elements provide a clue: nanoscale characterization of thin-film composite polyamide membranes. *ACS Appl. Mater. Interfaces* **7**, 16917–16922 (2015).
19. Wang, L. et al. Salt and water transport in reverse osmosis membranes: beyond the solution-diffusion model. *Environ. Sci. Technol.* **55**, 16665–16675 (2021).
20. González, M. P. et al. Effect of phosphoric and hydrofluoric acid on the structure and permeation of a nanofiltration membrane. *J. Memb. Sci.* **281**, 177–185 (2006).
21. Smith, B. C. Organic nitrogen compounds V: amine salts. https://www.spectroscopyonline.com/view/organic-nitrogen-compounds-v-amine-salts (2019).
22. Xu, R. et al. Influence of L-lysine on the permeation and antifouling performance of polyamide thin film composite reverse osmosis membranes. *RSC Adv.* **8**, 25236–25247 (2018).
23. Kamaly, N., Yameen, B., Wu, J. & Farokhzad, O. C. Degradable controlled-release polymers and polymeric nanoparticles: Mechanisms of controlling drug release. *Chem. Rev.* **116**, 2602–2663 (2016).
24. Zhao, Y., Zhang, Z., Dai, L. & Zhang, S. Preparation of high water flux and anti-fouling RO membranes using a novel diacyl chloride monomer with a phosphonate group. *J. Memb. Sci.* **536**, 98–107 (2017).
25. Rahimpour, A., Jahanshahi, M., Mortazavian, N., Madaeni, S. S. & Mansourpanah, Y. Preparation and characterization of asymmetric polyethersulfone and thin-film composite polyamide nanofiltration membranes for water softening. *Appl. Surf. Sci.* **256**, 1657–1663 (2010).
26. Sun, H. et al. Fabrication of thin-film composite polyamide nanofiltration membrane based on polyphenol intermediate layer with enhanced desalination performance. *Desalination* **488**, 114525 (2020).
27. Yu, S. et al. Study on polyamide thin-film composite nanofiltration membrane by interfacial polymerization of polyvinylamine (PVAm) and isophthaloyl chloride (IPC). *J. Memb. Sci.* **379**, 164–173 (2011).
28. Lee, J. S. et al. Simple method for preparing thin film composite polyamide nanofiltration membrane based on hydrophobic polyvinylidene fluoride support membrane. *Thin Solid Films* **624**, 136–143 (2017).
29. Wen, P. et al. Polyamide thin film composite nanofiltration membrane modified with acyl chlorided graphene oxide. *J. Memb. Sci.* **535**, 208–220 (2017).
30. Misdan, N., Lau, W. J., Ismail, A. F. & Matsuura, T. Formation of thin film composite nanofiltration membrane: Effect of polysulfone substrate characteristics. *Desalination* **329**, 9–18 (2013).
31. Li, W. et al. A positively charged composite nanofiltration membrane modified by EDTA for LiCl/MgCl2 separation. *Sep. Purif. Technol.* **186**, 233–242 (2017).
32. Ang, M. B. M. Y. et al. Correlating PSf support physicochemical properties with the formation of piperazine-based polyamide and evaluating the resultant nanofiltration membrane performance. *Polymers (Basel).* **9**, 505 (2017).
33. Jiang, Z. et al. A pH-stable positively charged composite nanofiltration membrane with excellent rejection performance. *RSC Adv.* **9**, 37546–37555 (2019).

ACKNOWLEDGEMENTS

Authors would like to acknowledge the support provided by the Interdisciplinary Research Center for Membranes and Water Security Project number # INMW2111, King Fahd University of Petroleum and Minerals, Saudi Arabia.

AUTHOR CONTRIBUTIONS

U.B.: conceptualization, investigation, visualization, data curation, methodology, writing—original draft, writing—review & editing and A.W.: conceptualization, investigation, visualization, data curation, methodology, writing—original draft, writing—review & editing.

COMPETING INTERESTS

The authors declare no competing interests.

ADDITIONAL INFORMATION

Supplementary information The online version contains supplementary material available at https://doi.org/10.1038/s41545-022-00186-x.

Correspondence and requests for materials should be addressed to Abdul Waheed.

Reprints and permission information is available at http://www.nature.com/reprints

Publisher's note Springer Nature remains neutral with regard to jurisdictional claims in published maps and institutional affiliations.